

Development and Evaluation of Novel Magnetic Actuated Microrobot with Spiral Motion Using Electromagnetic Actuation System

Qiang Fu¹ · Shuxiang Guo^{2,3} · Qiang Huang² · Hideyuki Hirata³ · Hidenori Ishihara³

Received: 2 April 2015 / Accepted: 13 October 2015 / Published online: 29 July 2016
© Taiwanese Society of Biomedical Engineering 2016

Abstract In this study, a magnetic spiral microrobot is proposed for tasks such as diagnosis, drug delivery, and minimally invasive surgery. It has a compact structure with a wireless power supply, low voltage, and a long working time. The microrobot is comprised of a spiral outer shell based on the Archimedes screw structure and an O-ring magnet for an actuator. The Archimedes screw structure produces an axial propulsive force due to the torsional moment generated by a magnetic field and embedded magnet, which rotates in the direction of interest. Microrobots with different numbers of spirals are manufactured to evaluate the effect of spiral number on speed. Moreover, we developed an electromagnetic actuation system to accomplish wireless real-time control via a Phantom Omni device. By adjusting the control signals, the microrobot achieved flexible motion in a pipe with good performance.

Keywords Magnetic spiral microrobot · Electromagnetic actuation system · Archimedes screw structure · Wireless power supply

1 Introduction

Microrobots have been employed in minimally invasive procedures due to their reliability and flexibility. They are safe and can perform tasks in small or narrow areas deep within the human body. Microrobots have many potential applications in the field of medical engineering [1–8]. With advances in precision processing technology, various microrobots with biomimetic locomotion have been developed, and further progress in the biomedical field is expected [6–12]. As a tool for diagnosis and treatment, microrobots can be used for tasks such as drug delivery and complex surgical operation [13–15]. Guo et al. developed several types of swimming microrobot using ionic conducting polymer film (ICPF) actuators that can swim like a fish with a tethered [16, 17]. They can move forward, float up or down, and steer left or right. However, fish-like microrobots are unsuitable for working inside the human body due to the requirement of a power cable. Given Imaging developed a kind of capsule endoscope (M2A) with a battery source that can be swallowed to examine the gastrointestinal (GI) tract based on the peristalsis of the intestines [18]. However, flexible motion cannot be performed via peristalsis. To solve this problem, self-propelled microrobots with biomimetic movements, such as crawling, walking, and creeping, have been developed. Motors or smart materials such as shape memory alloys, giant magnetostrictive alloys, ICPF, and piezoelectrics are utilized as actuators for self-propelled movement within

Electronic supplementary material The online version of this article (doi:10.1007/s40846-016-0147-7) contains supplementary material, which is available to authorized users.

✉ Qiang Fu
fuqiang252@gmail.com

✉ Shuxiang Guo
guoshuxiang@bit.edu.cn

¹ Graduate School of Engineering, Kagawa University, 2217-20 Hayashi-cho, Takamatsu, Kagawa 761-0396, Japan

² Key Laboratory of Convergence Medical Engineering System and Healthcare Technology, Ministry of Industry and Information Technology, Beijing Institute of Technology, Haidian District, Beijing 100081, China

³ Intelligent Mechanical Systems Engineering Department, Kagawa University, 2217-20 Hayashi-cho, Takamatsu, Kagawa 761-0396, Japan

the internal GI tract [19–22]. However, such microrobots do not have enough space to carry the battery source.

Magnetic microrobots are a popular choice because a magnetic field can provide wireless power for the microrobot to perform tasks. Several wireless magnetic microrobots that use different control methods have been developed. Honda et al. developed a wireless microrobot with a tail fin that can be controlled in only one direction [23]. Mei et al. developed a wireless microrobot driven by an intelligent magnetic material, obtaining desirable experimental results [24]. Pan and Guo developed a fish-like microrobot with a tail whose energy is provided by an oscillating uniform magnetic field [25–27]. Thomas et al. proposed the use of a non-uniform magnetic field emanating from a single rotating-permanent-magnet manipulator for the control of magnetic helical microrobots [28]. Yim et al. proposed a magnetically actuated soft capsule endoscope (MASCE) as a miniature mobile robot platform for medical diagnosis [29]. Magnetic microrobots are of great interest for microsurgery within the body of living organisms for minimally invasive medicine. Furthermore, the requirement of a wireless energy supply for swimming microrobots must be addressed to promote practical applications.

Microrobots driven by an electromagnetic actuation system that combines Helmholtz coils and Maxwell coils have recently been proposed [1]. These combined coils generally generate a gradient magnetic field that provides a propulsive force to the microrobot. The speed of the microrobot varies with the strength of the magnetic field (a larger magnetic field strength leads to higher speed). There are some limitations for clinical examination due to the relatively large volume and high energy consumption of

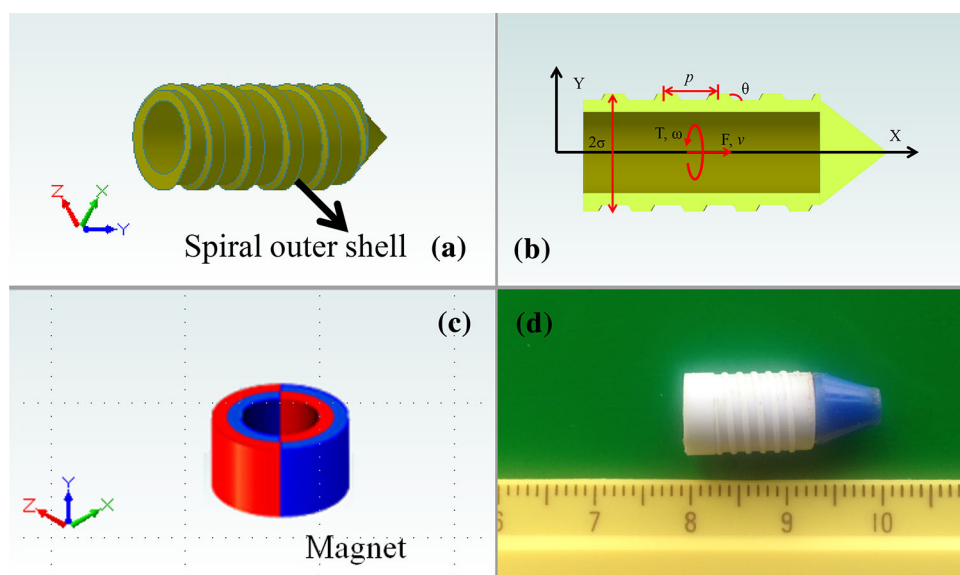
such microrobots. In the present study, three stationary Helmholtz coils are used to generate a uniform magnetic field to provide a propulsive force to the microrobot. The speed of the microrobot is controlled by adjusting the frequency of the magnetic field. The proposed electromagnetic actuation system has a relatively small volume and low embodied energy.

2 Materials and Methods

2.1 Structure of Magnetic Spiral Microrobot

During diagnosis and surgery, some factors such as, length of microrobot and diameter of microrobot, need be taken into account. Due to the overall limited size of microrobots, there is insufficient space for modules such as a camera module, a battery module, and a transmit/receive module. In addition, to accomplish medical tasks, a microrobot should be controlled by doctors. Therefore, a flexible, controllable, and wireless power supply is important for microrobots. To solve the above problems, we developed a self-propelled spiral microrobot manipulated by 3-axis Helmholtz coils, which generate an external orthogonally rotating magnetic field. The conceptual design of the magnetic spiral microrobot is shown in Fig. 1. The magnetic spiral microrobot is composed of a spiral outer shell based on the Archimedes screw structure and an O-ring magnet as an actuator. The Archimedes screw structure provides a propulsive force while the microrobot rotates using an external magnetic field. Due to the energy provided by the external magnetic field, the microrobot can work for a long time in the human body to accomplish

Fig. 1 **a** Structure, **b** model of magnetic spiral microrobot, **c** O-ring magnet, **d** Prototype of magnetic spiral microrobot



medical tasks. In addition, 50 % of the inner space is used to support tools for diagnosis. The prototype of the magnetic spiral microrobot is shown in Fig. 1d. The spiral outer shell is made of polythene plastic and is connected to the O-ring magnet by a strong adhesive. The specifications are given in Table 1.

2.2 Dynamic Model of Magnetic Spiral Microrobot

In this section, we build a dynamic model for the microrobot from a macroscopic viewpoint to analyze the force acting on the microrobot. Here, the dynamic model is based on two hypotheses: (1) the mean speed of motion relative to the fluid is low and constant; (2) the fluid is incompressible. Based on hydrodynamic theory, the motion states of the microrobot in a pipe are analyzed using the following equation:

Movement in the horizontal direction:

$$Ma = F_P - F_D \quad (1)$$

Movement in the vertical direction:

$$Ma = F_P - F_D \pm G \mp \rho gV \quad (2)$$

where M is the mass of the microrobot, a is the acceleration, F_P is the propulsive force, F_D is the total drag force, ρ is the density of the fluid, and G is the gravity force acting on the microrobot.

2.2.1 Propulsion Force on Magnetic Spiral Microrobot

The propulsive force of a magnetic spiral microrobot is along the central axis. In a low-Reynolds-number regime, the total applied nonfluidic torque and force are linearly related to the axial speed and angular speed with the parameters defined in Fig. 1b. The following symmetric propulsion matrix equation [30–32] is used to describe the propulsive force and torque of the magnetic spiral microrobot:

$$\begin{bmatrix} F \\ T \end{bmatrix} = \begin{bmatrix} a & b \\ c & d \end{bmatrix} \begin{bmatrix} v \\ \omega \end{bmatrix} \quad (3)$$

where F is the non-fluidic applied force, T is the non-fluidic applied torque, v is the axial speed, and ω is the angular

speed. We assume that the microrobot moves in water that has a constant density. k_1 and k_2 , which are the viscous drag coefficients for the magnetic spiral microrobot along and perpendicular to the axis, respectively, are constant. These two parameters are a theoretical maximum value that is related to parameters such as the radius of the microrobot, number of turns of the microrobot, and pitch of the microrobot [30, 31]. From the symmetric propulsion matrix, the speed of the microrobot is a function of the geometric parameters. The matrix parameters a , b , and c are calculated as:

$$\left. \begin{aligned} a &= 6.2n\sigma \left(\frac{k_1 \cos^2 \theta + k_2 \sin^2 \theta}{\sin \theta} \right) \\ b &= 6.2n\sigma(k_1 - k_2) \cos \theta \\ c &= b \\ d &= 6.2n\sigma \left(\frac{k_2 \cos^2 \theta + k_1 \sin^2 \theta}{\sin \theta} \right) \end{aligned} \right\} \quad (4)$$

where k_1 and k_2 are the constants defined above and n is the number of turns of the microrobot.

2.2.2 Fluid Drag Force on Magnetic Spiral Microrobot

The total drag force depends on the Reynolds number and the shape of the magnetic spiral microrobot. In a pipe, the Reynolds number is generally defined as:

$$Re = \frac{\rho v d}{\mu} \quad (5)$$

The total drag force can be expressed as:

$$F_D = C_D \frac{1}{2} \rho v^2 S + \mu_f N \quad (6)$$

where ρ is the density of the fluid, v is the speed of the microrobot, d is the diameter of the microrobot, μ is the coefficient of kinematic viscosity, S is the maximum cross area that is vertical to the flow of fluid, C_D is the resistance coefficient, μ_f is the coefficient of friction, and N is the normal force between the microrobot and the surface of the pipe.

2.2.3 Mechanical Efficiency

When the magnetic spiral microrobot moves from point A to point B, the total work done (W) on the microrobot by the propulsive force and the drag force equals the change in kinetic energy (ΔK), expressed as:

$$W = \int_A^B dW = \int_A^B \bar{F} \cdot d\vec{r} = \Delta K \quad (7)$$

In the ideal case, the propulsive force is converted into kinetic energy. If the speed of the microrobot is changed,

Table 1 Specifications of magnetic spiral microrobot

Length of microrobot	20 mm
Radius of microrobot	8 mm
Weight of microrobot	2.306 g
Magnetization direction	Radial
Radius of magnet	6 mm
Weight of the microrobot	1.036 g
Material of body	Polythene

the kinetic energy of the object is changed as well. In reality, some of the energy is converted into thermal energy due to the drag force. According to the law of conservation of energy, the ideal case of kinetic energy (K_i) and the real case of kinetic energy (K_r) are calculated respectively as:

$$\Delta K_i = \frac{1}{2}mv_{iB}^2 - \frac{1}{2}mv_{iA}^2 \tag{8}$$

$$\Delta K_r = \frac{1}{2}mv_{rB}^2 - \frac{1}{2}mv_{rA}^2 \tag{9}$$

The mechanical efficiency η is calculated as:

$$\eta = \frac{\Delta K_r}{\Delta K_i} \times 100\% \tag{10}$$

where v_{iA} and v_{iB} are the microrobot’s speeds at points A and B in the ideal case, and v_{rA} and v_{rB} are the microrobot’s speeds at points A and B in a real case, respectively.

2.3 Control Principle of Microrobot Using Rotating Magnetic Field

2.3.1 Magnetic Force and Magnetic Torque

When a rotating magnetic field is applied to the plane normal to the axis of the spiral, the magnet rotates due to magnetic torque (T_m). Ampere’s law indicates that the magnetic force (F_m) integrated along any closed path is equal to the total current enclosed by that path. Therefore, wherever there is current flow, there is a corresponding magnetic force. The magnetic force and magnetic torque acting on the O-ring magnet in the external magnetic field of the 3-axis Helmholtz coils are respectively given as [33]:

$$F_m = \mu_0 V(M \cdot \nabla)B = (F_{mx}, F_{my}, F_{mz}) \tag{11}$$

$$T_m = \mu_0 VM \times B = (T_{mx}, T_{my}, T_{mz}) \tag{12}$$

where μ_0 is the permeability of free space, M and V are the average magnetization and the volume of the O-ring magnet, respectively, and B is the magnet flux density.

The torque (τ) required to rotate the microrobot with angular speed is given as:

$$\omega = 2\pi f \tag{13}$$

$$\tau = D(\omega) + E(\omega) \tag{14}$$

where $D(\omega)$ is the torque for the O-ring magnet and $E(\omega)$ is the torque for the spiral. According to the equation above, if the magnetic flux density is increased, the magnetism and torque will increase. If the torque T_m becomes equal to the required rotational torque of the magnetic spiral microrobot τ , the magnetic spiral microrobot will move in the water. The speed of the microrobot increases with increasing angular speed of the magnetic spiral.

2.3.2 Locomotion Principle with Rotating Magnetic Field

Based on magnetic theory, the magnetic spiral microrobot rotates inside the magnetic field due to the torsional moment. In this study, a 3-axis Helmholtz coil is used to generate a symmetric rotating magnetic field. The magnetic field can rotate the embedded inner O-ring magnet with radial magnetization to produce an axial propulsive force. The control and locomotion principle of one step cycle are described in Fig. 2a. When coils HX and HY are controlled by the two sinusoidal wave channels, which have the same frequency and a 90° phase difference (Fig. 2b), a symmetric rotating magnetic field is generated in the pipe (Fig. 2c), and rotating motion is achieved. As the water pushes backward, the microrobot moves forward via the reaction force. By changing the rotation direction of the symmetric magnetic field, the microrobot can move backward. In addition, the speed of the microrobot can be adjusted by changing the frequency of the control signals.

2.3.3 Rotating Magnetic Fields

In our previous study [4], we operated the microrobot using an alternating magnetic field only in the horizontal direction. However, this is not sufficient for practical applications. Thus, we designed a device with 3-axis Helmholtz coils. Each axial coil generates a magnetic field in one direction. By combining three magnetic fields together, we can create a magnetic field in any direction. The resulting magnetic field is used to provide the magnetic force and the magnetic torque for the microrobot. According to Ampere’s law and the Biot-Savart law, the resulting magnetic field can be defined as [33]:

$$B = \begin{bmatrix} B_x \\ B_y \\ B_z \end{bmatrix} = \begin{bmatrix} a \cos(\omega t) \cos \alpha & 0 & 0 \\ 0 & b \cos(\omega t) \cos \gamma & 0 \\ 0 & 0 & c \cos(\omega t) \cos \beta \end{bmatrix} \begin{bmatrix} I_x \\ I_y \\ I_z \end{bmatrix} \tag{15}$$

where $B_x(t)$, $B_y(t)$, and $B_z(t)$ denote the magnetic flux densities of the x-, y- and z-axes, respectively; α , β , and γ denote the angles between the moving direction of the microrobot and the x-, y-, and z-axes, respectively; and a , b , and c are constants of the three Helmholtz coils, respectively.

3-axis Helmholtz coils were fabricated. The radius, number of turns, and resistance for each coil are given in Table 2. In order to precisely control the wireless capsule microrobot in three-dimensional (3D) space, the 3-axis Helmholtz coils were characterized using the software

Fig. 2 Locomotion principle of magnetic spiral microrobot. *Yellow arrow* indicates magnetic field direction at current time. *Green arrow* indicates rotation direction. **a** One step cycle of forward motion, **b** control signals of coils, and **c** symmetric rotating magnetic field

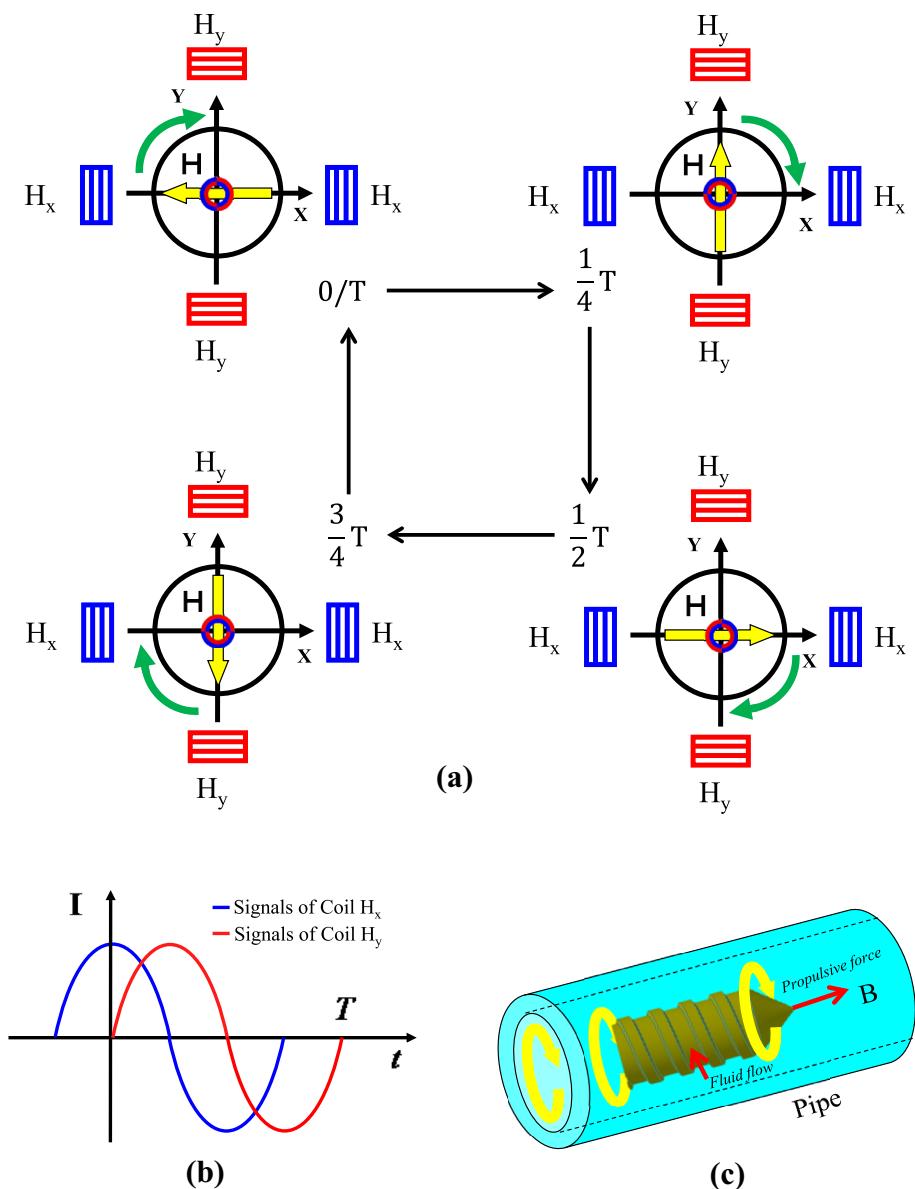


PHOTO-Series version 7.1 (PHOTON Co. Ltd.). When $B_x = 1 \text{ mT}$, $B_y = 0 \text{ mT}$, and $B_z = 0 \text{ mT}$, the 3-axis Helmholtz coils generated a magnetic field along the x-axis. By changing the values of B_x , B_y , and B_z , the 3-axis Helmholtz coils generated a magnetic field along any direction. These results confirm that a 3D magnetic field can be generated using the proposed coil system. Moreover, we analyzed the magnetic flux density of the 3-axis Helmholtz coils using the finite element method and measured the magnetic flux density using a gauss meter (TESLA METER TM-701). The gauss meter was placed in the workspace of the 3-axis Helmholtz coils. Then, the magnetic flux density was measured from the boundary to the center with a step length of 10 mm and a current of 0 to 3 A. The simulation result of the magnetic flux density in

Table 2 Specifications of 3-axis Helmholtz coils

	H_x	H_y	H_z
Coil radius (mm)	142	175	200
Coil length (mm)	142	175	200
Number of turns	125	150	180
Resistance (Ω)	2.4	3.3	4.5
Material	Cu	Cu	Cu

the workspace is 0.83 mT/A, which is consistent with the measured value of 0.81 mT/A. The measurement results indicate that the magnetic flux density is linearly proportional to current. We can thus control the magnetic flux

density of each Helmholtz coil (B_x , B_y , and B_z) by adjusting the current of each Helmholtz coil to control the movement direction of the microrobot.

3 Results and Discussion

To achieve wireless real-time control of the microrobot, a microrobotic control system is proposed [33]. It includes a data acquisition board (USB-4716, Advantech, China), a DC power supply, a control unit, 3-axis Helmholtz coils, an oscilloscope, a Phantom Omni device (SensAble), a web camera, a pipe, and a personal computer. The microrobot was placed in a transparent pipe (inner diameter: 26 mm; thickness: 3 mm) filled with water. The control signals were applied to the 3-axis Helmholtz coils in order to obtain a rotating magnetic field via the data acquisition board and control unit. The magnetic flux density and the magnetic field frequency were adjusted using the Phantom Omni device. The web camera was used to monitor the inside of the pipe. During experiments, the Phantom Omni device was used to control the position and posture of the microrobot with the help of a display. The display showed data used for obtaining the real-time position of the robot. The oscilloscope showed the magnetic flux density changing frequency.

3.1 Evaluation of Magnetic Microrobot Characteristics

The hydrodynamic models in Sect. 2 indicate that the forward speed increases with angular speed and number of spirals. The movement of the microrobot depends on the magnetic flux density and the number of spirals of the microrobot. Therefore, we evaluated the performance of the microrobot with various spiral numbers and magnetic flux densities.

In experiment I, two types of magnetic spiral microrobot, with the same spiral height, spiral width, and spiral angles, but different numbers of spirals (5 and 10, respectively), were tested. The pitches of the microrobots were different. The speed was measured for a given magnetic field. By adjusting the frequency of the control signal from 0 to 20 Hz and keeping the amplitude of the input currents fixed at 3 A, the mean speeds were measured with a laser sensor (KEYENCE LK-800). The relationship between the magnetic flux density changing frequency and the speed of the microrobot is shown in Fig. 3. The experimental results show that the speed increases with increasing magnetic flux density changing frequency and number of spirals. The microrobot with ten spiral numbers performs better than the microrobot with five spiral numbers, especially for high rotation speeds.

In experiment II, the speed of the magnetic spiral microrobot was measured for various magnetic flux densities. The magnetic flux density changing frequency was adjusted from 0 to 20 Hz and the speed was measured. The relationship between the speed and the magnetic flux density changing frequency is shown in Fig. 4. The red and blue lines are the mean speeds of the microrobot for magnetic flux densities of 2.4 and 2 mT, respectively. The results show that the propulsive force of the spiral microrobot does not depend on the magnitude of the magnetic flux density when the driving frequency is lower than a step-out frequency.

In experiment III, the bi-directional relationship between the magnetic flux density changing frequency and the speed was investigated. The results, shown in Fig. 5a, show that in the frequency range of 0–15 Hz, the microrobot can rotate continuously, synchronized with the rotating magnetic fields, and generate enough propulsion to overcome the resistance of fluids. In the frequency range of 15–20 Hz, the microrobot can no longer rotate continuously. The frequency of 15 Hz is called a step-out frequency. The step-out frequency is related to the microrobot's weight, magnetic torque, and any other loads. This frequency is well understood for magnetic spiral microrobots in uniform magnetic fields and is discussed in our previous research [33]. The experimental results indicate a linear relation between magnetic field changing frequencies and speed in the range of 0–15 Hz. At 15 Hz, the maximum speed is 11.8 mm/s in the horizontal direction and 3.64 mm/s in the vertical direction. Figure 5b shows the relationship between the rotational frequency and the speed of the magnetic spiral microrobot in the

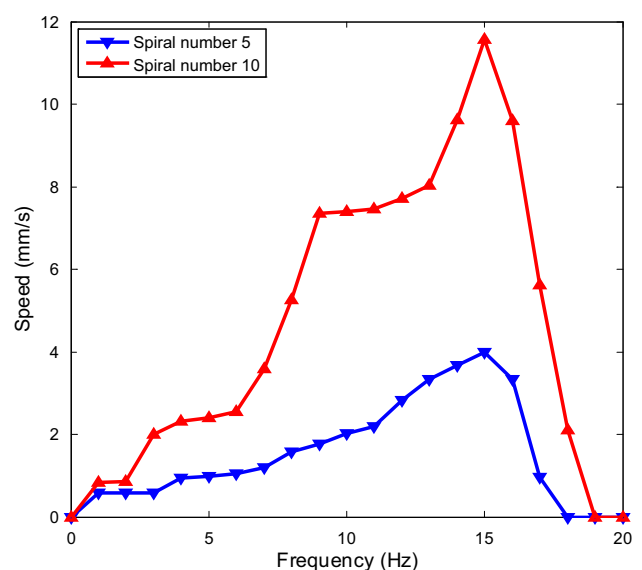


Fig. 3 Measurement results for various spiral numbers

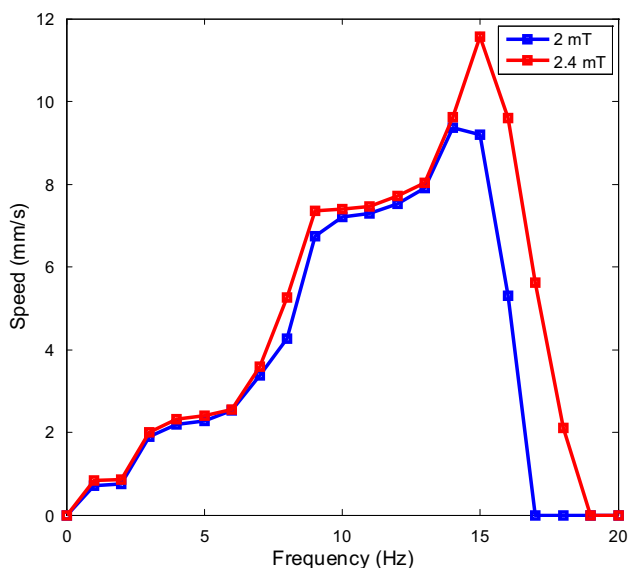


Fig. 4 Relationship between magnetic flux density changing frequency and speed

vertical direction. This disparity of the experimental result between the Fig. 5a, b is due to the extra force needed to overcome gravity (see Sect. 2).

3.2 Real Time Control

The Phantom Omni device sends control instructions to the 3-axis Helmholtz coils, which produce a changing frequency of the magnetic flux density to control the movement of the wireless microrobot in the pipe. The principle

speed control of the wireless microrobot according to changing the rotating direction of the Phantom Omni device handle is detailed [9]. When the angle between the handle and the y-axis is 0° or 90° , the wireless microrobot obtains its minimum speed ($speed_{\min}$) and maximum speed ($speed_{\max}$), respectively. When the rotational direction of the handle is counter-clockwise or clockwise, the wireless microrobot speeds up and slows down, respectively. By adjusting the rotational direction of the handle, we can control the speed of the wireless microrobot.

During the experiment, the rotational angle of the handle was changed from 0° to 90° , which generated a frequency from 0 to 15 Hz. When the rotational angle of the handle was changed from 0° to 90° , the microrobot accelerated. When it was changed from 90° to 0° , the microrobot decelerated. When the rotational angle of the handle was 0° , the wireless microrobot became motionless.

3.3 Navigation of Microrobot

Figure 6 shows the variable speed motion in the pipe. The microrobot moves in the pipe at 1, 5, and 15 Hz, and then stops. It then moves in the pipe at 15 and 5 Hz respectively, and then stops. In the experiments of rotational motion, the microrobot was controlled to rotate with a certain angle for some time. A curve of rotation angle versus time is shown in Fig. 7.

Overall, the experimental results show that the magnetic spiral microrobot moves when a low magnetic flux density is applied. By changing the rotation direction of the symmetric magnetic field generated by 3-axis Helmholtz coils,

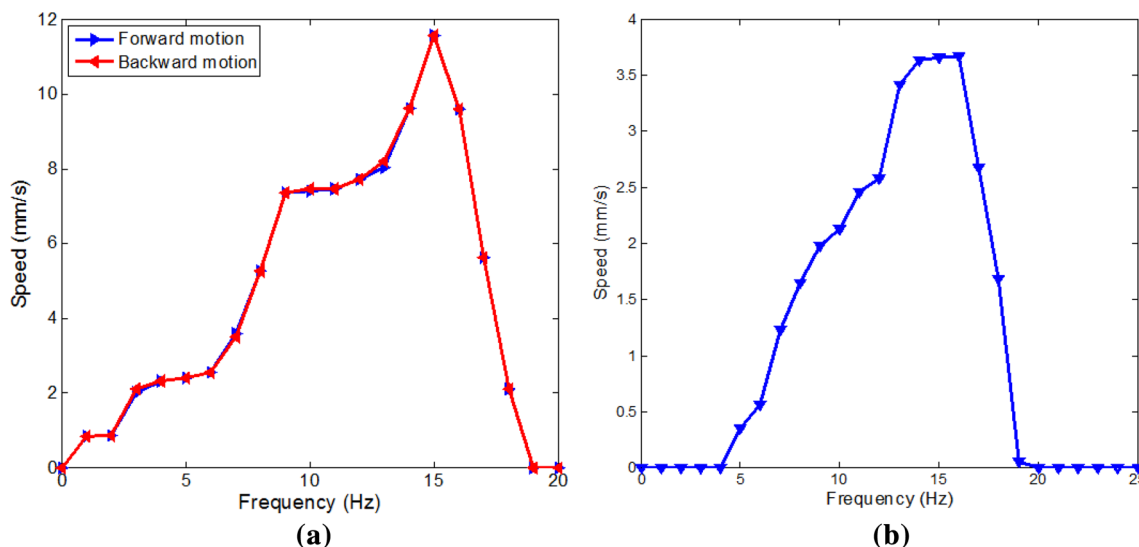


Fig. 5 **a** Bi-directional relationship between magnetic flux density changing frequency and speed. **b** Relationship between magnetic flux density changing frequency and speed in vertical direction

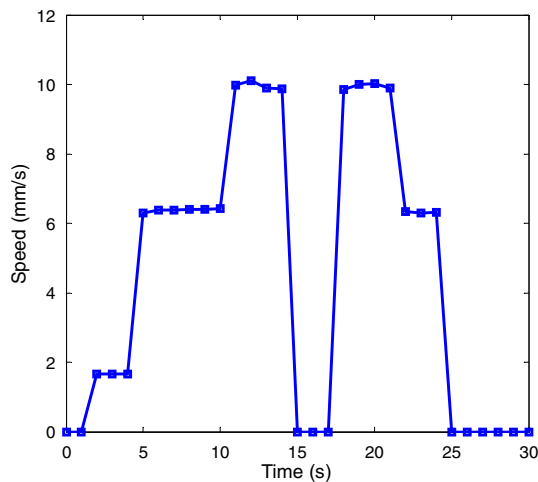


Fig. 6 Experimental results of variable motion

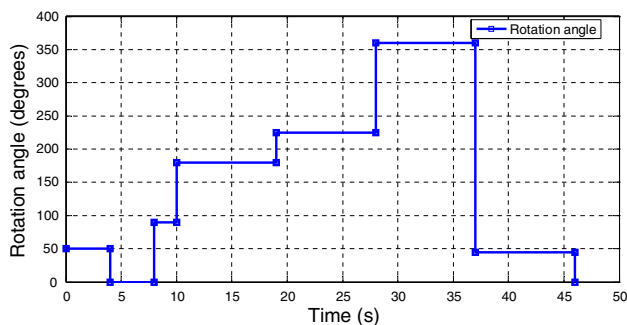


Fig. 7 Rotation angle of microrobot

the magnetic spiral microrobot can move forward and backward. By adjusting the frequency of the control signals, the magnetic spiral microrobot can accelerate, decelerate, and stop.

4 Conclusion

This study proposed a magnetic spiral microrobot with a magnetic actuator that can be loaded with diagnostic tools, such as a camera. To control the wireless microrobot, 3-axis Helmholtz coils generate a rotating magnetic field. We evaluated the performance of the rotating magnetic field and the characteristics of the wireless microrobot with various magnetic flux density changing frequencies and spiral numbers. Based on the experimental results, we designed an experiment to control the wireless microrobot in real-time using a Phantom Omni device. By adjusting the magnetic field changing frequency and the rotational magnetic field direction, the wireless microrobot was made to move in various directions. The magnetic spiral microrobot performed very well. In future studies, the

microrobot can be fitted with devices for medical purposes. In addition, the design and energy supply of the wireless microrobot will be optimized further, leading to useful medical applications.

Acknowledgments This research was partly supported by the National Natural Science Foundation of China (61375094), Key Research Program of the Natural Science Foundation of Tianjin (13JCZDJC26200), National High-Tech Research and Development Program of China (2015AA043202), JSPS KAKENHI (grant 15K2120), and Kagawa University Characteristic Prior Research Fund 2015.

References

1. Yu, C., Kim, J., Choi, H., Choi, J., Jeong, S., Cha, K., et al. (2010). Novel electromagnetic actuation system for three-dimensional locomotion and drilling of intravascular microrobot. *Sensors and Actuators A: Physical*, *161*, 297–304.
2. Onogi, S., Nakajima, Y., Koyama, T., Tamura, Y., Kobayashi, E., Sakuma, I., et al. (2013). Robotic vertebral puncture system for percutaneous vertebroplasty. *Journal of Medical and Biological Engineering*, *33*, 491–496.
3. Rodríguez, A. B., Ramirez, A. R. G., Pieri, E. R. D., Lopez, A. L., & Albornoz, A. D. C. D. (2012). An approach for robot-based odor navigation. *Journal of Medical and Biological Engineering*, *32*, 453–456.
4. Pan, Q., Guo, S., & Okada, T. (2011). A novel hybrid wireless microrobot. *International Journal of Mechatronics and Automation*, *1*, 60–69.
5. Khamesee, M. B., Kato, N., Nomura, Y., & Nakamura, T. (2002). Design and control of a microrobotic system using magnetic levitation. *IEEE-ASME Transactions on Mechatronics*, *7*, 1–14.
6. Abbott, J. J., Erganeman, O., Kummer, M., Hirt, A., & Nelson, B. J. (2007). Modeling magnetic torque and force for controlled manipulation of soft-magnetic bodies. *IEEE Transactions on Robotics*, *23*, 1247–1251.
7. Yesin, K. B., Vollmers, K., & Nelson, B. J. (2006). Modeling and control of untethered biomicrorobots in a fluidic environment using electromagnetic fields. *International Journal of Robotics Research*, *25*, 527–536.
8. Arcese, L., Fruchard, M., & Ferreira, A. (2013). Adaptive controller and observer for a magnetic microrobot. *IEEE Transactions on Robotics*, *29*, 1060–1067.
9. Fu, Q., Guo, S., & Yamauchi, Y. (2014). A control system of the wireless microrobots in pipe. In *Proceedings of IEEE International Conference on Mechatronics and Automation* (pp. 1995–2000).
10. Lee, J. S., Kim, B., & Hong, Y. S. (2009). A flexible chain-based screw propeller for capsule endoscopes. *The International Journal of Precision Engineering and Manufacturing*, *10*, 27–34.
11. Choi, H., Choi, J., Jeong, S., Yu, C., Park, J., & Park, S. (2009). Two dimensional locomotion of microrobot with novel stationary electromagnetic actuation system. *Smart Materials and Structures*, *18*, 1–6.
12. Yu, M. (2002). M2A™ capsule endoscopy—A breakthrough diagnostic tool for small intestine imaging. *Gastroenterology Nursing*, *25*, 24–27.
13. Peyer, K. E., Zhang, L., & Nelson, B. J. (2013). Bio-inspired magnetic swimming microrobots for biomedical applications. *Nanoscale*, *5*, 1259–1272.
14. Kim, S. H., & Ishiyama, K. (2014). Magnetic robot and manipulation for active-locomotion with targeted drug release. *IEEE-ASME Transactions on Mechatronics*, *19*, 1651–1659.

15. Choi, K., Jang, G., Jeon, S., & Nam, J. (2014). Capsule-type magnetic microrobot actuated by an external magnetic field for selective drug delivery in human blood vessels. *IEEE Transactions on Magnetics*, *50*, 1–4.
16. Guo, S., Fukuda, T., & Asaka, K. (2002). Fish-like underwater microrobot with 3 DOF. In *Proceedings of IEEE International Conference on Robotics and Automation* (pp. 738–743)
17. Guo, S., Fukuda, T., & Asaka, K. (2003). A new type of fish-like underwater microrobot. *IEEE-ASME Transactions on Mechatronics*, *8*, 136–141.
18. Moglia, A., Menciassi, A., Schurr, M. O., & Dario, P. (2007). Wireless capsule endoscopy: From diagnostic devices to multi-purpose robotic systems. *Biomedical Microdevices*, *9*, 235–243.
19. Rentschler, M. E., & Oleynikov, D. (2007). Recent in vivo surgical robot and mechanism developments. *Surgical Endoscopy*, *21*, 1477–1481.
20. Gao, B., Guo, S., & Ye, X. (2011). Motion-control analysis of ICPF-actuated underwater biomimetic microrobots. *International Journal of Mechatronics and Automation*, *1*, 79–89.
21. Kim, B., Lee, S., Park, J. H., & Park, J. O. (2005). Design and fabrication of a locomotive mechanism for capsule-type endoscopes using shape memory alloys (SMAs). *IEEE-ASME Transactions on Mechatronics*, *10*, 77–86.
22. Fukuda, T., Hosokai, H., Ohyama, H., Hashimoto, H., & Arai, F. (1991). Giant magnetostrictive alloy (GMA) applications to micro mobile robot as a micro actuator without power supply cables. In *Micro structures, sensors, actuators, machines and robots* (pp. 210–215)
23. Honda, T., Sakashita, T., Narahashi, K., & Yamasaki, J. (2001). Swimming properties of bending-type magnetic micro-machine. *Journal Magnetics Society of Japan*, *4*, 1175–1178.
24. Mei, T., Chen, Y., Fu, G., & Kong, D. (2002). Wireless drive and control of a swimming microrobot. In *Proceedings of IEEE international conference on robotics and automation* (pp. 1131–1136)
25. Pan, Q., & Guo, S. (2007) Mechanism and control of a novel type of microrobot for biomedical application. In *Proceedings of IEEE international conference on robotics and automation* (pp. 187–192)
26. Guo, S., Pan, Q., & Khamesee, M. B. (2008). Development of a novel type of microrobot for biomedical application. *Microsystem Technologies*, *14*, 307–314.
27. Pan, Q., & Guo, S. (2009). A paddling type of microrobot in pipe. In *Proceedings of IEEE international conference on robotics and automation* (pp. 2995–3000)
28. Fountain, T. W. R., Kailat, P. V., & Abbott, J. J. (2010) Wireless control of magnetic helical microrobots using a rotating-permanent-magnet manipulator. In *Proceedings of IEEE international conference on robotics and automation* (pp. 576–581)
29. Yim, S., & Sitti, M. (2012). Design and rolling locomotion of a magnetically actuated soft capsule endoscope. *IEEE Transactions on Robotics*, *28*, 183–193.
30. Abbott, J. J., Peyer, K. E., Lagomarsino, M. C., Zhang, L., Dong, L., Kaliakatsos, I. K., et al. (2009). How should microrobots swim? *International Journal of Robotics Research*, *28*, 1434–1447.
31. Purcell, E. M. (1977). Life at low Reynolds number. *American Journal of Physics*, *45*, 3–11.
32. Brennen, C., & Winet, H. (1977). Fluid mechanics of propulsion by cilia and flagella. *Annual Review of Fluid Mechanics*, *9*, 339–398.
33. Fu, Q., Guo, S., Yamauchi, Y., Hirata, H., & Ishihara, H. (2015). A novel hybrid microrobot using rotational magnetic field for medical applications. *Biomedical Microdevices*, *17*, 1–12.